A mixed-contact formulation for a dynamics simulation of flexible systems: an integration with model-reduction techniques

Blaž Starc, Gregor Čepon, Miha Boltežar

January 12, 2017

Cite as:
Blaž Starc, Gregor Čepon and Miha Boltežar.
A mixed-contact formulation for a dynamics simulation of flexible systems: an integration with model-reduction techniques. Journal of Sound and Vibration. In Press. Accepted manuscript, available online: 12-JAN-2017
DOI: 10.1016/j.jsv.2017.01.026

Abstract

A new numerical procedure for efficient dynamics simulations of linear-elastic systems with unilateral contacts is proposed. The method is based on the event-driven integration of a contact problem with a combination of single- and set-valued force laws together with classical model-reduction techniques. According to the contact state, the developed event-driven integration enables the formulation of reduced system matrices. Moreover, to enable the transition among different reduced spaces the formulation of the initial conditions is also presented. The method has been developed separately for each of the four most popular model-reduction techniques (Craig-Bampton, MacNeal, Rubin and Dual Craig-Bampton). The applicability of the newly presented method is demonstrated on a simple clamped-beam structure with a unilateral contact, which is excited with a harmonic force at the free end.

1 Introduction

Numerical investigations of systems represent a common engineering technique to reduce the costs of an end-product. The dynamic analysis of systems is usually conducted by applying a dense mesh and using the classical finite-element method. As the refinement of the finite elements increases, a large computational effort is required to solve systems with a large number of Degrees of Freedom (DoF). This is especially the case when a transient time response is required, due to the usually high stiffness of mechanical systems, which implies small time-steps during the integration. Another well-known problem is the modelling of contacts between flexible bodies [1, 2, 3, 4, 5]. These contacts introduce non-linearities and add a high stiffness in the contact region, which further decreases the required time-step. This often leads to long computation times that require enormous computational resources.

The model-reduction techniques [6] are well known methods that address the large number of DoF. They reduce the system matrices, but retain the essential information for the analyses. They are mostly used for analysing small deformations and vibration phenomena. In the case of the system response, they also make possible significantly faster integration times, due to the reduced number of Equations of Motion (EoM). The most common methods are the Craig-Bampton method [7] (1968), MacNeal [8] (1971), Rubin [9] (1975), Craig-Chang [10] (1977) and the Dual Craig-Bampton method [11] (2004). A practical case and a comparison of the methods can be found in [12]. In recent years, in addition to the classical linear model-reduction techniques, the non-linear model-reduction techniques have also attracted a lot of scientific attention [13]. They enable the modelling of non-linearities, such as large deformations, local non-linearities, non-linear damping or coupling effects, for instance the analysis of jointed structures [14].

The modelling of contacts between flexible bodies is usually formulated using the penalty method [5] or more advanced methods that introduce a non-penetration condition [15, 16]. By using the penalty method, a large penalty factor may lead to an ill-conditioned stiffness matrix and consequently to a poor convergence. On the other hand, the method that imposes a non-penetration condition originates from the contact formulation between rigid bodies [5, 17]. The first studies were made on rigid-body unilateral contacts in the form of the linear complementarity problem (LCP) and were published by Lötstedt [18]. In the framework of non-smooth contact dynamics, Moreau [19] introduced a numerical treatment of rigid bodies with unilateral contacts, Coulomb friction and impacts. Without any significant change to the computational strategies Jean [20] applied a method to treat the contacts between flexible bodies. In comparison to time-stepping methods, the event-driven methods integrate the dynamical system until the event occurs. In [21], Čepon and Boltežar proposed a mixed-contact formulation between flexible bodies using event-driven integration together with the penalty method. The method models the impact with the penalty method, while the continuous contact is modelled by a Lagrange-multipliers method. In the recent years newer methods have emerged, which present a more advanced (non-linear) contact model. Willner [22] and Goerke and Willner [23] present an iterative elastic half-space solution based on a variational principle. A simple modification also enables the approximative solution of the elasto-plastic contact, which is modelled with a power-law relationship between the pressure and the contact gap. Arz and Laville [24] presented an impact model that is based on a system of two equations: Newton's second law and the non-linear viscoelastic contact force law, originally presented in [25]. Pohrt and Popov [26] observed a non-linear behaviour of the contact normal stiffness, which is in a power-law dependence with the normal force. Furthermore, they also observed power-like dependencies on the rms value of the roughness, the elastic modulus and the nominal area of contact. The power-law dependence was confirmed experimentally by Zhai *et al* [27]. Kostek [28] presented a non-linear contact model describing the hysteresis of a dry contact for rough surfaces loaded in the normal direction. The model also accounts for the plastic defor-

mation of the virgin contact as well as the insensibility of the contact hysteresis to the frequency of the loading. Ahmadian and Mohammadali [29] consider the hysteresis effects in both normal and shear contact directions. The model is rate independent and represents coupling effects between normal and shear displacements and is based on power-law dependence between the normal/shear force and the displacement.

In this paper a new method is proposed that enables efficient dynamics simulations of linear-elastic systems with unilateral contacts. The method proposes the integration of a contact formulation, as presented in [21] together with classical modal-reduction techniques. According to the contact state, the developed event-driven integration scheme enables the formulation of reduced system matrices. The updating algorithm for the static and vibration modes is therefore in direct correlation with the changing boundary DoF during the system response. It is shown that the reduction basis for the continuous and the impact contact formulation can be obtained based on a flexible system without contacts. Moreover, to enable the transition among different reduced spaces the formulation of the initial conditions is also presented. The method has been developed separately for each of the four most popular model-reduction techniques (Craig-Bampton, MacNeal, Rubin and Dual Craig-Bampton). The applicability of the newly presented method is demonstrated on a simple clamped-beam structure with a unilateral contact, which is excited by a harmonic force at the free end.

The article is organised as follows. The second section presents the four classical model-reduction techniques. The third section presents the event-driven integration of reduced models with unilateral contacts. The new definitions of the system matrices, the initial conditions and the events are defined according to the contact state. The fourth section presents a case study of a clamped beam with a unilateral contact, together with the advantages of the proposed method. In the last section a summary and the contributions are presented.

2 Model reduction techniques

Model-reduction techniques [30] are efficient methods to reduce the size of large finite-element method (FEM) models. They retain the dense finite-element mesh, but replace the physical degrees of freedom with a much smaller set of generalised degrees of freedom. This is done by modal superposition and truncation. The methods can be divided into two main groups [31]: fixed- and free-interface methods. The most known fixed-interface method is the Craig-Bampton method [7], and the free-interface methods are MacNeal [8], Rubin [9] and Dual Craig-Bampton [11]. A good overall step-by-step description of the methods can be found in [12]. The methods consist of a reduction basis containing static modes and a limited number of vibration modes. The static modes can be further divided into the constraint, attachment and residual attachment modes. The vibration modes are divided into the free-interface, rigid-body and fixed interface modes. Hence, the fixed/free-interface methods are determined by the selection of the vibration modes and the accompanying static modes.

A detailed description of the above-mentioned modes is found in [12], [32] and [31].

The model-reduction techniques are closely connected to the substructuring field, where a substructure dynamical model is defined as:

$$\mathbf{M}^{(s)}\,\ddot{\mathbf{u}}^{(s)}(t) + \mathbf{C}^{(s)}\,\dot{\mathbf{u}}^{(s)}(t) + \mathbf{K}^{(s)}\,\mathbf{u}^{(s)}(t) = \mathbf{f}^{(s)}(t) + \mathbf{g}^{(s)}(t), \tag{1}$$

The matrices $\mathbf{M}^{(s)}$, $\mathbf{C}^{(s)}$ and $\mathbf{K}^{(s)}$ represent the mass, the damping and the stiffness matrix of a substructure s, $\mathbf{u}^{(s)}(t)$ is the displacement vector, $\mathbf{f}^{(s)}(t)$ is the external excitation vector and $\mathbf{g}^{(s)}(t)$ is the vector of connection forces with the surrounding substructures.

The next step is to divide the physical DoF $\mathbf{u}$ into the internal $\mathbf{u}_\mathrm{i}$ and the boundary DoF $\mathbf{u}_\mathrm{b}$. Moreover, the damping is assumed to be small and can therefore be neglected during the reduction process. If necessary, the damping matrix can be later introduced in the from of a simple damping model, such as the Rayleigh, or proposing the modal damping. This gives Eq. (1) the following shape:

$$\begin{bmatrix} \mathbf{M}_\mathrm{ii} & \mathbf{M}_\mathrm{ib} \\ \mathbf{M}_\mathrm{bi} & \mathbf{M}_\mathrm{bb} \end{bmatrix} \begin{Bmatrix} \ddot{\mathbf{u}}_\mathrm{i} \\ \ddot{\mathbf{u}}_\mathrm{b} \end{Bmatrix} + \begin{bmatrix} \mathbf{K}_\mathrm{ii} & \mathbf{K}_\mathrm{ib} \\ \mathbf{K}_\mathrm{bi} & \mathbf{K}_\mathrm{bb} \end{bmatrix} \begin{Bmatrix} \mathbf{u}_\mathrm{i} \\ \mathbf{u}_\mathrm{b} \end{Bmatrix} = \begin{Bmatrix} \mathbf{f}_\mathrm{i} \\ \mathbf{f}_\mathrm{b} \end{Bmatrix} + \begin{Bmatrix} \mathbf{g}_\mathrm{i} \\ \mathbf{g}_\mathrm{b} \end{Bmatrix}, \tag{2}$$

where the index i denotes the internal DOF and b denotes the boundary DOF. Note that the internal excitation forces $\mathbf{g}_\mathrm{i}$ are assumed to be $\mathbf{0}$, since there is no contact with the neighbouring substructures.

The reduction process uses the division of the DoF (Eq. 2) in order to derive the system matrices. A description of the fixed- and free-interface methods is given below.

2.1 Fixed-interface methods

The fixed-interface methods are represented by approximating the internal displacements $\mathbf{u}_\mathrm{i}$ with fixed-interface modes $\mathbf{\Phi}_\mathrm{i}$ and the corresponding static modes $\mathbf{\Psi}$:

$$\mathbf{u}_\mathrm{i} \approx \mathbf{\Psi}_\mathrm{c}\,\mathbf{u}_\mathrm{b} + \mathbf{\Phi}_\mathrm{i}\,\boldsymbol{\eta}_\mathrm{i} \tag{3}$$

Here, $\mathbf{\Psi}_\mathrm{c}$ are the static constraint modes, which are used in the Craig-Bampton method. $\mathbf{\Phi}_\mathrm{i}$ are a reduced set of fixed-interface vibration modes with the corresponding modal DOF $\boldsymbol{\eta}_\mathrm{i}$. Hence, the reduction basis is the following:

$$\begin{Bmatrix} \mathbf{u}_\mathrm{i} \\ \mathbf{u}_\mathrm{b} \end{Bmatrix} \approx \begin{bmatrix} \mathbf{\Phi}_\mathrm{i} & \mathbf{\Psi}_\mathrm{c} \\ \mathbf{0} & \mathbf{I} \end{bmatrix} \begin{Bmatrix} \boldsymbol{\eta}_\mathrm{i} \\ \mathbf{u}_\mathrm{b} \end{Bmatrix} = \mathbf{R}_\mathrm{CB}\,\mathbf{q}_\mathrm{CB} \tag{4}$$

If Eq. (4) is inserted into Eq. (2) and the orthogonality between the vibration modes with respect to the mass or stiffness matrix [32] is taken into account, the following reduced equations of motion are obtained:

$$\begin{bmatrix} \mathbf{I} & \mathbf{M}_{\phi\mathrm{b}} \\ \mathbf{M}_{\mathrm{b}\phi} & \tilde{\mathbf{M}}_\mathrm{bb} \end{bmatrix} \begin{Bmatrix} \ddot{\boldsymbol{\eta}}_\mathrm{i} \\ \ddot{\mathbf{u}}_\mathrm{b} \end{Bmatrix} + \begin{bmatrix} \mathbf{\Omega}_\mathrm{i}^2 & \mathbf{0} \\ \mathbf{0} & \tilde{\mathbf{K}}_\mathrm{bb} \end{bmatrix} \begin{Bmatrix} \boldsymbol{\eta}_\mathrm{i} \\ \mathbf{u}_\mathrm{b} \end{Bmatrix} = \begin{Bmatrix} \tilde{\mathbf{f}}_\mathrm{i} \\ \tilde{\mathbf{f}}_\mathrm{b} \end{Bmatrix} + \begin{Bmatrix} \mathbf{0} \\ \mathbf{g}_\mathrm{b} \end{Bmatrix}, \tag{5}$$

where:

$$\begin{aligned}
\tilde{\mathbf{K}}_{\mathrm{bb}} &= \mathbf{K}_{\mathrm{bb}} - \mathbf{K}_{\mathrm{bi}}\,\mathbf{K}_{\mathrm{ii}}^{-1}\,\mathbf{K}_{\mathrm{ib}} \\
\tilde{\mathbf{M}}_{\mathrm{bb}} &= \mathbf{M}_{\mathrm{bb}} - \mathbf{M}_{\mathrm{bi}}\,\mathbf{K}_{\mathrm{ii}}^{-1}\,\mathbf{K}_{\mathrm{ib}} - \mathbf{K}_{\mathrm{bi}}\,\mathbf{K}_{\mathrm{ii}}^{-1}\,\mathbf{M}_{\mathrm{ib}} + \mathbf{K}_{\mathrm{bi}}\,\mathbf{K}_{\mathrm{ii}}^{-1}\,\mathbf{M}_{\mathrm{ii}}\,\mathbf{K}_{\mathrm{ii}}^{-1}\,\mathbf{K}_{\mathrm{ib}} = \\
&= \mathbf{M}_{bb} - \mathbf{M}_{\mathrm{bi}}\,\boldsymbol{\Psi}_{\mathrm{c}} - \boldsymbol{\Psi}_{\mathrm{c}}^{\mathrm{T}}\,\mathbf{M}_{\mathrm{ib}} + \boldsymbol{\Psi}_{\mathrm{c}}^{\mathrm{T}}\,\mathbf{M}_{\mathrm{ii}}\,\boldsymbol{\Psi}_{\mathrm{c}} \\
\mathbf{M}_{\phi\mathrm{b}} &= \boldsymbol{\Phi}_{\mathrm{i}}^{\mathrm{T}}(\mathbf{M}_{\mathrm{ib}} - \mathbf{M}_{\mathrm{ii}}\,\mathbf{K}_{\mathrm{ii}}^{-1}\,\mathbf{K}_{\mathrm{ib}}) \\
\mathbf{M}_{\mathrm{b}\phi} &= \mathbf{M}_{\phi\mathrm{b}}^{\mathrm{T}} \\
\tilde{\mathbf{f}}_{\mathrm{i}} &= \boldsymbol{\Phi}_{\mathrm{i}}^{\mathrm{T}}\,\mathbf{f}_{\mathrm{i}} \\
\tilde{\mathbf{f}}_{\mathrm{b}} &= \mathbf{f}_{\mathrm{b}} - \mathbf{K}_{\mathrm{bi}}\,\mathbf{K}_{\mathrm{ii}}^{-1}\,\mathbf{f}_{\mathrm{i}} = \boldsymbol{\Psi}_{\mathrm{c}}^{\mathrm{T}}\,\mathbf{f}_{\mathrm{i}}
\end{aligned} \tag{6}$$

Here, $\boldsymbol{\Omega}_{\mathrm{i}}^2$ represents a diagonal matrix of squared fixed-interface frequencies $\omega_{\mathrm{i},j}^2$.

2.2 Free-interface methods

The free-interface methods' reduction consists of reducing the displacement vector $\mathbf{u}$ by the free-interface modes $\boldsymbol{\Phi}_{\mathrm{f}}$, the rigid-body modes $\boldsymbol{\Phi}_{\mathrm{r}}$ and the corresponding static modes $\boldsymbol{\Psi}$. Here, the residual attachment modes $\boldsymbol{\Psi}_{\mathrm{r}}$ are used, which serve as a basis for the Rubin, MacNeal and Dual Craig-Bampton methods.

2.2.1 Rubin and MacNeal methods

Both the Rubin [9] and MacNeal methods [8] have the same reduction basis containing free-interface modes $\boldsymbol{\Phi}_{\mathrm{f}}$ with the corresponding modal DOF $\boldsymbol{\eta}_{\mathrm{f}}$, rigid-body modes $\boldsymbol{\Phi}_{\mathrm{r}}$ with the corresponding modal DOF $\boldsymbol{\eta}_{\mathrm{r}}$ and residual attachment modes $\boldsymbol{\Psi}_{\mathrm{r}}$. They approximate the displacement vector as:

$$\mathbf{u} \approx \boldsymbol{\Psi}_{\mathrm{r}}\,\mathbf{g}_{\mathrm{b}} + \boldsymbol{\Phi}_{\mathrm{r}}\,\boldsymbol{\eta}_{\mathrm{r}} + \boldsymbol{\Phi}_{\mathrm{f}}\,\boldsymbol{\eta}_{\mathrm{f}} \tag{7}$$

Inserting Eq. (7) into Eq. (1) and accounting for the orthogonality between the vibration modes, the rigid-body modes and their combination [32], gives the following form:

$$\begin{bmatrix} \mathbf{I} & \mathbf{0} & \mathbf{0} \\ \mathbf{0} & \mathbf{I} & \mathbf{0} \\ \mathbf{0} & \mathbf{0} & \mathbf{M}_{\mathrm{r,bb}} \end{bmatrix} \begin{Bmatrix} \ddot{\boldsymbol{\eta}}_{\mathrm{r}} \\ \ddot{\boldsymbol{\eta}}_{\mathrm{f}} \\ \ddot{\mathbf{g}}_{\mathrm{b}} \end{Bmatrix} + \begin{bmatrix} \mathbf{0} & \mathbf{0} & \mathbf{0} \\ \mathbf{0} & \boldsymbol{\Omega}_{\mathrm{f}}^2 & \mathbf{0} \\ \mathbf{0} & \mathbf{0} & \mathbf{G}_{\mathrm{r,bb}} \end{bmatrix} \begin{Bmatrix} \boldsymbol{\eta}_{\mathrm{r}} \\ \boldsymbol{\eta}_{\mathrm{f}} \\ \mathbf{g}_{\mathrm{b}} \end{Bmatrix} = \begin{Bmatrix} \boldsymbol{\Phi}_{\mathrm{r}}^{\mathrm{T}} \\ \boldsymbol{\Phi}_{\mathrm{f}}^{\mathrm{T}} \\ \boldsymbol{\Psi}_{\mathrm{r}}^{\mathrm{T}} \end{Bmatrix} \mathbf{f} + \begin{Bmatrix} \boldsymbol{\Phi}_{\mathrm{r}}^{\mathrm{T}} \\ \boldsymbol{\Phi}_{\mathrm{f}}^{\mathrm{T}} \\ \boldsymbol{\Psi}_{\mathrm{r}}^{\mathrm{T}} \end{Bmatrix} \mathbf{g} \tag{8}$$

where:

$$\begin{aligned}
\mathbf{G}_{\mathrm{r,bb}} &= \boldsymbol{\Psi}_{\mathrm{r}}^{\mathrm{T}}\,\mathbf{K}\,\boldsymbol{\Psi}_{\mathrm{r}} = \mathbf{A}\,\mathbf{G}_{\mathrm{r}}\,\mathbf{A}^{\mathrm{T}} \\
\mathbf{M}_{\mathrm{r,bb}} &= \boldsymbol{\Psi}_{\mathrm{r}}^{\mathrm{T}}\,\mathbf{M}\,\boldsymbol{\Psi}_{\mathrm{r}}
\end{aligned} \tag{9}$$

$\mathbf{A}$ is a boolean matrix selecting the interface DOF and $\mathbf{G}_{\mathrm{r}}$ is the residual flexibility matrix, which is obtained from the residual attachment modes [12, 31]. Both methods apply a second transformation in order to transform the interface force DOF $\mathbf{g}_{\mathrm{b}}$ to the interface displacements $\mathbf{u}_{\mathrm{b}}$. This involves pre-multiplying Eq. (7) by the boolean matrix $\mathbf{A}$:

$$\mathbf{u}_{\mathrm{b}} = \mathbf{A}\,\mathbf{u} = \mathbf{A}(\boldsymbol{\Psi}_{\mathrm{r}}\,\mathbf{g}_{\mathrm{b}} + \boldsymbol{\Phi}_{\mathrm{r}}\,\boldsymbol{\eta}_{\mathrm{r}} + \boldsymbol{\Phi}_{\mathrm{f}}\,\boldsymbol{\eta}_{\mathrm{f}}) = \mathbf{G}_{\mathrm{r,bb}}\,\mathbf{g}_{\mathrm{b}} + \boldsymbol{\Phi}_{\mathrm{r|b}}\,\boldsymbol{\eta}_{\mathrm{r}} + \boldsymbol{\Phi}_{\mathrm{f|b}}\,\boldsymbol{\eta}_{\mathrm{f}}. \tag{10}$$

Here the subscript $_{|\mathrm{b}}$ indicates the dependence on the boundary DOFs, which were selected by the boolean matrix $\mathbf{A}$ (e.g. $\mathbf{\Phi}_{\mathrm{r}|\mathrm{b}} = \mathbf{A}\,\mathbf{\Phi}_{\mathrm{r}}$). The second transformation is defined by exposing the interface force $\mathbf{g}_{\mathrm{b}}$ from Eq. (10) and by writing it into the DOF vector:

$$\left\{ \begin{array}{c} \boldsymbol{\eta}_{\mathrm{r}} \\ \boldsymbol{\eta}_{\mathrm{f}} \\ \mathbf{g}_{\mathrm{b}} \end{array} \right\} = \left[\begin{array}{ccc} \mathbf{I} & \mathbf{0} & \mathbf{0} \\ \mathbf{0} & \mathbf{I} & \mathbf{0} \\ -\mathbf{K}_{\mathrm{r,bb}}\,\mathbf{\Phi}_{\mathrm{r}|\mathrm{b}} & -\mathbf{K}_{\mathrm{r,bb}}\,\mathbf{\Phi}_{\mathrm{f}|\mathrm{b}} & \mathbf{K}_{\mathrm{r,bb}} \end{array} \right] \left\{ \begin{array}{c} \boldsymbol{\eta}_{\mathrm{r}} \\ \boldsymbol{\eta}_{\mathrm{f}} \\ \mathbf{u}_{\mathrm{b}} \end{array} \right\} \tag{11}$$

Note that $\mathbf{K}_{\mathrm{r,bb}} = \mathbf{G}_{\mathrm{r,bb}}^{-1}$. The Rubin method is defined by inserting Eq. (11) into Eq. (8) and the Rubin reduced equations of motion are obtained:

$$\left[\begin{array}{ccc} \mathbf{I} + \mathbf{\Phi}_{\mathrm{r}|\mathrm{b}}^{\mathrm{T}}\,\overline{\mathbf{M}}_{\mathrm{r}}\,\mathbf{\Phi}_{\mathrm{r}|\mathrm{b}} & \mathbf{\Phi}_{\mathrm{r}|\mathrm{b}}^{\mathrm{T}}\,\overline{\mathbf{M}}_{\mathrm{r}}\,\mathbf{\Phi}_{\mathrm{f}|\mathrm{b}} & -\mathbf{\Phi}_{\mathrm{r}|\mathrm{b}}^{\mathrm{T}}\,\overline{\mathbf{M}}_{\mathrm{r}} \\ \mathbf{\Phi}_{\mathrm{f}|\mathrm{b}}^{\mathrm{T}}\,\overline{\mathbf{M}}_{\mathrm{r}}\,\mathbf{\Phi}_{\mathrm{r}|\mathrm{b}} & \mathbf{I} + \mathbf{\Phi}_{\mathrm{f}|\mathrm{b}}^{\mathrm{T}}\,\overline{\mathbf{M}}_{\mathrm{r}}\,\mathbf{\Phi}_{\mathrm{f}|\mathrm{b}} & -\mathbf{\Phi}_{\mathrm{f}|\mathrm{b}}^{\mathrm{T}}\,\overline{\mathbf{M}}_{\mathrm{r}} \\ -\overline{\mathbf{M}}_{\mathrm{r}}\,\mathbf{\Phi}_{\mathrm{r}|\mathrm{b}} & -\overline{\mathbf{M}}_{\mathrm{r}}\,\mathbf{\Phi}_{\mathrm{f}|\mathrm{b}} & \overline{\mathbf{M}}_{\mathrm{r}} \end{array} \right] \left\{ \begin{array}{c} \ddot{\boldsymbol{\eta}}_{\mathrm{r}} \\ \ddot{\boldsymbol{\eta}}_{\mathrm{f}} \\ \ddot{\mathbf{u}}_{\mathrm{b}} \end{array} \right\} +$$

$$\left[\begin{array}{ccc} \mathbf{\Phi}_{\mathrm{r}|\mathrm{b}}^{\mathrm{T}}\,\mathbf{K}_{\mathrm{r,bb}}\,\mathbf{\Phi}_{\mathrm{r}|\mathrm{b}} & \mathbf{\Phi}_{\mathrm{r}|\mathrm{b}}^{\mathrm{T}}\,\mathbf{K}_{\mathrm{r,bb}}\,\mathbf{\Phi}_{\mathrm{f}|\mathrm{b}} & -\mathbf{\Phi}_{\mathrm{r}|\mathrm{b}}^{\mathrm{T}}\,\mathbf{K}_{\mathrm{r,bb}} \\ \mathbf{\Phi}_{\mathrm{f}|\mathrm{b}}^{\mathrm{T}}\,\mathbf{K}_{\mathrm{r}}\,\mathbf{\Phi}_{\mathrm{r}|\mathrm{b}} & \mathbf{\Omega}_{\mathrm{f}}^2 + \mathbf{\Phi}_{\mathrm{f}|\mathrm{b}}^{\mathrm{T}}\,\mathbf{K}_{\mathrm{r,bb}}\,\mathbf{\Phi}_{\mathrm{f}|\mathrm{b}} & -\mathbf{\Phi}_{\mathrm{f}|\mathrm{b}}^{\mathrm{T}}\,\mathbf{K}_{\mathrm{r,bb}} \\ -\mathbf{K}_{\mathrm{r,bb}}\,\mathbf{\Phi}_{\mathrm{r}|\mathrm{b}} & -\mathbf{K}_{\mathrm{r,bb}}\,\mathbf{\Phi}_{\mathrm{f}|\mathrm{b}} & \mathbf{K}_{\mathrm{r,bb}} \end{array} \right] \left\{ \begin{array}{c} \boldsymbol{\eta}_{\mathrm{r}} \\ \boldsymbol{\eta}_{\mathrm{f}} \\ \mathbf{u}_{\mathrm{b}} \end{array} \right\} = \tag{12}$$

$$\left\{ \begin{array}{c} \tilde{\mathbf{f}}_{\mathrm{r}} \\ \tilde{\mathbf{f}}_{\mathrm{f}} \\ \tilde{\mathbf{f}}_{\mathrm{b}} \end{array} \right\} + \left\{ \begin{array}{c} \mathbf{0} \\ \mathbf{0} \\ \mathbf{g}_{\mathrm{b}} \end{array} \right\}$$

where:

$$\begin{aligned} \overline{\mathbf{M}}_{\mathrm{r}} &= \mathbf{K}_{\mathrm{r,bb}}\,\mathbf{M}_{\mathrm{r,bb}} \\ \tilde{\mathbf{f}}_{\mathrm{r}} &= (\mathbf{\Phi}_{\mathrm{r}}^{\mathrm{T}} - \mathbf{\Phi}_{\mathrm{r}|\mathrm{b}}^{\mathrm{T}}\,\mathbf{K}_{\mathrm{r,bb}}\,\mathbf{\Psi}_{\mathrm{r}}^{\mathrm{T}})\mathbf{f} \\ \tilde{\mathbf{f}}_{\mathrm{f}} &= (\mathbf{\Phi}_{\mathrm{f}}^{\mathrm{T}} - \mathbf{\Phi}_{\mathrm{f}|\mathrm{b}}^{\mathrm{T}}\,\mathbf{K}_{\mathrm{r,bb}}\,\mathbf{\Psi}_{\mathrm{r}}^{\mathrm{T}})\mathbf{f} \\ \tilde{\mathbf{f}}_{\mathrm{b}} &= \mathbf{K}_{\mathrm{r,bb}}\,\mathbf{\Psi}_{\mathrm{r}}^{\mathrm{T}}\,\mathbf{f} \end{aligned} \tag{13}$$

The Rubin reduction basis can therefore be defined as follows:

$$\left\{ \begin{array}{c} \mathbf{u}_{\mathrm{i}} \\ \mathbf{u}_{\mathrm{b}} \end{array} \right\} \approx \left[\begin{array}{ccc} \mathbf{\Phi}_{\mathrm{r}|\mathrm{i}} - \mathbf{\Psi}_{\mathrm{r}|\mathrm{i}}\,\mathbf{K}_{\mathrm{r,bb}}\,\mathbf{\Phi}_{\mathrm{r}|\mathrm{b}} & \mathbf{\Phi}_{\mathrm{f}|\mathrm{i}} - \mathbf{\Psi}_{\mathrm{r}|\mathrm{i}}\,\mathbf{K}_{\mathrm{r,bb}}\,\mathbf{\Phi}_{\mathrm{f}|\mathrm{b}} & \mathbf{\Psi}_{\mathrm{r}|\mathrm{i}}\,\mathbf{K}_{\mathrm{r,bb}} \\ \mathbf{0} & \mathbf{0} & \mathbf{I} \end{array} \right] \left\{ \begin{array}{c} \boldsymbol{\eta}_{\mathrm{r}} \\ \boldsymbol{\eta}_{\mathrm{f}} \\ \mathbf{u}_{\mathrm{b}} \end{array} \right\} = \mathbf{R}_{\mathrm{R}}\,\mathbf{q}_{\mathrm{R}} \tag{14}$$

The MacNeal method differs from the Rubin method in neglecting the residual mass term $\mathbf{M}_{\mathrm{r,bb}}$ in Eq. (8), with the same procedure afterwards.

2.2.2 Dual Craig-Bampton method

The Dual Craig-Bampton method (DCB) [11] is a newer method (2004) and uses the same approximation basis as the Rubin and MacNeal methods in Eq. (7). However, where the Rubin and MacNeal methods employ the second transformation, the DCB method keeps the interface forces as part of the generalized DOF. Hence, the assembly procedure is later different compared to the other three methods. The reduction basis is written as:

$$\left\{ \begin{array}{c} \mathbf{u} \\ \mathbf{g}_{\mathrm{b}} \end{array} \right\} \approx \left[\begin{array}{ccc} \mathbf{\Phi}_{\mathrm{r}} & \mathbf{\Phi}_{\mathrm{f}} & \mathbf{\Psi}_{\mathrm{r}} \\ \mathbf{0} & \mathbf{0} & \mathbf{I} \end{array} \right] \left\{ \begin{array}{c} \boldsymbol{\eta}_{\mathrm{r}} \\ \boldsymbol{\eta}_{\mathrm{f}} \\ \mathbf{g}_{\mathrm{b}} \end{array} \right\} = \mathbf{R}_{\mathrm{DCB}}\,\mathbf{q}_{\mathrm{DCB}} \tag{15}$$

The substructure equations of motion are written as:

$$\begin{bmatrix} \mathbf{M} & \mathbf{0} \\ \mathbf{0} & \mathbf{0} \end{bmatrix} \begin{Bmatrix} \ddot{\mathbf{u}} \\ \ddot{\mathbf{g}}_\mathrm{b} \end{Bmatrix} + \begin{bmatrix} \mathbf{K} & -\mathbf{A}^\mathrm{T} \\ -\mathbf{A} & \mathbf{0} \end{bmatrix} \begin{Bmatrix} \mathbf{u} \\ \mathbf{g}_\mathrm{b} \end{Bmatrix} = \begin{Bmatrix} \mathbf{f} \\ \mathbf{0} \end{Bmatrix} + \begin{Bmatrix} \mathbf{0} \\ -\mathbf{u}_\mathrm{b} \end{Bmatrix} \tag{16}$$

The second row in Eq. (16) is added to enforce the compatibility during assembly. When Eq. (15) is inserted in Eq. (16) the following Dual Craig-Bampton reduced equations of motion are obtained:

$$\begin{bmatrix} \mathbf{I} & \mathbf{0} & \mathbf{0} \\ \mathbf{0} & \mathbf{I} & \mathbf{0} \\ \mathbf{0} & \mathbf{0} & \mathbf{M}_{\mathrm{r,bb}} \end{bmatrix} \begin{Bmatrix} \ddot{\boldsymbol{\eta}}_\mathrm{r} \\ \ddot{\boldsymbol{\eta}}_\mathrm{f} \\ \ddot{\mathbf{g}}_\mathrm{b} \end{Bmatrix} + \begin{bmatrix} \mathbf{0} & \mathbf{0} & -\boldsymbol{\Phi}_{\mathrm{r|b}}^\mathrm{T} \\ \mathbf{0} & \boldsymbol{\Omega}_\mathrm{f}^2 & -\boldsymbol{\Phi}_{\mathrm{f|b}}^\mathrm{T} \\ -\boldsymbol{\Phi}_{\mathrm{r|b}} & -\boldsymbol{\Phi}_{\mathrm{f|b}} & -\mathbf{G}_{\mathrm{r,bb}} \end{bmatrix} \begin{Bmatrix} \boldsymbol{\eta}_\mathrm{r} \\ \boldsymbol{\eta}_\mathrm{f} \\ \mathbf{g}_\mathrm{b} \end{Bmatrix} = \begin{Bmatrix} \boldsymbol{\Phi}_\mathrm{r}^\mathrm{T}\mathbf{f} \\ \boldsymbol{\Phi}_\mathrm{f}^\mathrm{T}\mathbf{f} \\ \boldsymbol{\Psi}_\mathrm{r}^\mathrm{T}\mathbf{f} \end{Bmatrix} - \begin{Bmatrix} \mathbf{0} \\ \mathbf{0} \\ \mathbf{u}_\mathrm{b} \end{Bmatrix} \tag{17}$$

3 Contact formulation

In general, contacts can be modelled as single-valued or set-valued force laws. The single-valued force law assumes a flexible contact region and is described using smooth functions. Here, a unilateral contact is proposed, where the linear contact force λ_U is defined as:

$$\lambda_\mathrm{U} = \begin{Bmatrix} 0, & u_\mathrm{U} \geq 0 \\ \max(0, -(k\,u_\mathrm{U} + d\,\dot{u}_\mathrm{U})), & u_\mathrm{U} < 0 \end{Bmatrix}, \tag{18}$$

where k is the penalty stiffness, d is the penalty damping, u_U is the relative displacement and $\dot{u}_\mathrm{U}$ is the relative velocity. Figure 1a presents the unilateral force law for a zero relative velocity $\dot{u}_\mathrm{U} = 0$. Note that the single-valued force laws are sometimes also referred to as the penalty formulation, due to the use of a spring and a damper, which introduces the contact force.

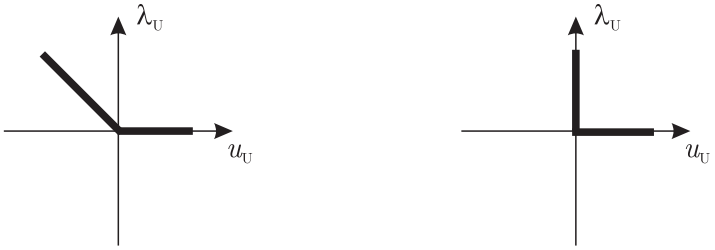

(a) (b)

Figure 1: Linear force laws for unilateral contacts: a) Single-valued, b) Set-valued.

The unilateral set-valued force law is shown in Fig. 1b. Recent studies also show the possibility to model a contact between flexible systems with set-valued force laws [33]. Here, the combination of the single-valued and the set-valued unilateral force law is proposed in order to describe the contact between reduced models obtained using the model-reduction techniques. The formulation

enables an evaluation of the impact forces using the well-known penalty law and a description of the continuous contacts using the augmented Lagrange approach. Three different contact states can be identified (Fig. 2): **no-contact**, **continuous** and **impact/penalty**. Each contact state requires a derivation of its own reduction basis; therefore, the mass and stiffness matrices are not unique during the integration process.

Figure 2: Contact formulations: a) No-contact, b) Continuous, c) Impact/Penalty.

While the transition from a no-contact to an impact/penalty contact formulation is straightforward, the transition from impact/penalty to continuous contact is required in order to avoid numerical problems. Usually, the penalty laws are represented by stiff linear or non-linear springs, which often lead to ill-conditioned systems of differential equations. Hence, the procedure presented in Fig. 3 is proposed in order to overcome these problems.

When the impact occurs a certain penetration is allowed, as shown in Fig. 3. As the penalty law includes a dissipative component after a period of time, the normal velocity is close to zero. Now, the contact can be classified as continuous and the Augmented Lagrangian approach is applied in order to avoid an ill-conditioned system. The transition from the continuous to the no-contact state occurs when the adhesive force is detected between the contacting bodies.

The presented contact formulation requires a derivation of the reduced spaces for each individual contact state, as well as the derivation of the new initial conditions to enable a transition among them. The contact formulation for the four most popular model-reduction techniques is presented in more detail.

3.1 System response of a reduced model with contacts

The computation of the system response of a reduced model consists of an event-driven integration, which switches among three contact states (see Fig. 3): no-contact, continuous and impact/penalty models. The three models can all be derived from the no-contact model. The continuous model is defined by setting the constrained DoF to zero. Hence, the corresponding rows and columns in the mass, stiffness and damping matrices are zero. Similarly, the penalty model uses the no-contact model by adding a penalty weight to the corresponding coordinate in the stiffness and damping matrices ($\mathbf{K}_{\mathrm{bb}}$ in Eq. (2)). Note, Rayleigh damping is used to obtain the damping matrices.

Apart from models, the events also need to be redefined for the reduced model (see Fig. 3). The constraint forces for the continuous contact state are

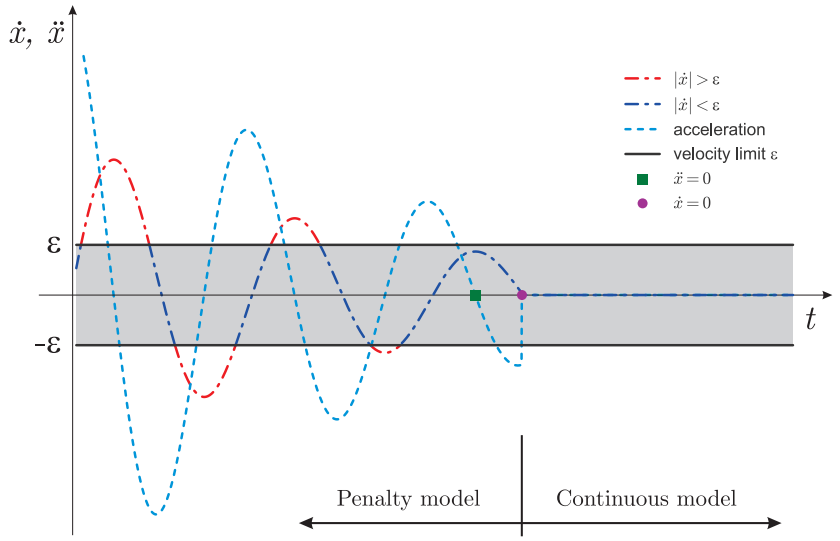

Figure 3: Events within penalty method

obtained from the no-contact model (Eq. (2)):

$$\mathbf{g}_\mathrm{b} = \mathbf{M}_\mathrm{bi}\,\ddot{\mathbf{u}}_\mathrm{i} + \mathbf{M}_\mathrm{bb}\,\ddot{\mathbf{u}}_\mathrm{b} + \mathbf{K}_\mathrm{bi}\,\mathbf{u}_\mathrm{i} + \mathbf{K}_\mathrm{bb}\,\mathbf{u}_\mathrm{b} - \mathbf{f}_\mathrm{b} \tag{19}$$

Since the boundary displacements and accelerations are zero, Eq. 19 is simplified to:

$$\mathbf{g}_\mathrm{b} = \mathbf{M}_\mathrm{bi}\,\ddot{\mathbf{u}}_\mathrm{i} + \mathbf{K}_\mathrm{bi}\,\mathbf{u}_\mathrm{i} - \mathbf{f}_\mathrm{b} \tag{20}$$

When using model-reduction techniques, the constraint force Eq. (20) as well as the penalty/impact system matrices must be formulated for the model-reduction techniques in the following way:

a) Craig-Bampton method

The penalty-method stiffness matrix is modified only in the $\tilde{\mathbf{K}}_\mathrm{bb}$ part (see Eqs. (5) and (6)). The remaining reduced matrices are unchanged.

The constraint force for the reduced case is deduced from Eqs. (5) and (20):

$$\mathbf{g}_\mathrm{b} = \mathbf{M}_\mathrm{b\phi}\,\ddot{\boldsymbol{\eta}}_\mathrm{i} + \mathbf{M}_\mathrm{bb}\,\ddot{\mathbf{u}}_\mathrm{b} + \mathbf{K}_\mathrm{bb}\,\mathbf{u}_\mathrm{b} - \tilde{\mathbf{f}}_\mathrm{b} \tag{21}$$

and since the boundary displacements and accelerations are zero, the equation further reduces to:

$$\mathbf{g}_\mathrm{b} = \mathbf{M}_\mathrm{b\phi}\,\ddot{\boldsymbol{\eta}}_\mathrm{i} - \tilde{\mathbf{f}}_\mathrm{b} \tag{22}$$

b) MacNeal, Rubin and Dual Craig-Bampton methods

The penalty stiffness matrix and force vector are modified in all the terms, since $\mathbf{K}_\mathrm{bb}$ is in all of the matrix parts (see Eq. (12)). The re-computation

of $\mathbf{K}_{\mathrm{r,bb}}$ and $\overline{\mathbf{M}}_{\mathrm{r}}$ and their dot products with free-interface, rigid-body and residual-attachment modes is required. Using the Rubin method, the mass matrix also needs to be recomputed. With the Dual Craig-Bampton method this procedure is simpler, since only $\mathbf{K}_{\mathrm{r,bb}}$ and $\mathbf{M}_{\mathrm{r,bb}}$ need to be recomputed in the mass and stiffness matrices (see Eq. (17)).

The constraint force for all three methods is defined with Eq. (11). The equation can be simplified due to the zero boundary displacements and accelerations:

$$\mathbf{g}_{\mathrm{b}} = -\mathbf{K}_{\mathrm{r,bb}}\,\boldsymbol{\Phi}_{\mathrm{r|b}}\,\boldsymbol{\eta}_{\mathrm{r}} - \mathbf{K}_{\mathrm{r,bb}}\,\boldsymbol{\Phi}_{\mathrm{f|b}}\,\boldsymbol{\eta}_{\mathrm{f}} \tag{23}$$

The constraint force in Eq. (22) and Eq. (23) is used to compute the constraint force of the continuous model. Note that the constraint force in the penalty model is computed with the use of a single-valued unilateral constraint (Eq. (18)). An important aspect presented in the calculation of a system response for a reduced model is the calculation of newly defined initial conditions, in order to enable a smooth transition among the reduced spaces.

3.2 Derivation of new initial conditions for a reduced system

The computation of the new initial conditions between two modal spaces is done through the physical coordinates. Therefore, the modal coordinates need to be first transformed to physical coordinates and afterwards to the new modal space. Since the boundary DoFs are usually preserved in the physical space, only the internal DoFs need to be transformed:

$$\mathbf{u}_{\mathrm{i,\,old}} = \mathbf{u}_{\mathrm{i,\,new}} \tag{24}$$

In our case the **old** ($_{\mathrm{old}}$) and **new** ($_{\mathrm{new}}$) coordinates are represented by the **no-contact**, **continuous** and **penalty** models. The derivation for different model-reduction methods differs due to different reduced spaces. A detailed description is given below.

3.2.1 Craig-Bampton method

The Craig-Bampton modal space is given by its reduction matrix in Eq. (4). The comparison of the new and old internal displacement DoFs then results in:

$$\boldsymbol{\Phi}_{\mathrm{i,\,new}}\,\boldsymbol{\eta}_{\mathrm{i,\,new}} + \boldsymbol{\Psi}_{\mathrm{c,\,new}}\,\mathbf{u}_{\mathrm{b,\,new}} = \boldsymbol{\Phi}_{\mathrm{i,\,old}}\,\boldsymbol{\eta}_{\mathrm{i,\,old}} + \boldsymbol{\Psi}_{\mathrm{c,\,old}}\,\mathbf{u}_{\mathrm{b,\,old}} \tag{25}$$

The new (no-contact) modal space is therefore defined as:

$$\boldsymbol{\eta}_{\mathrm{i,\,new}} = \boldsymbol{\Phi}^{+}_{\mathrm{i,\,new}}(\boldsymbol{\Phi}_{\mathrm{i,\,old}}\,\boldsymbol{\eta}_{\mathrm{i,\,old}} + \boldsymbol{\Psi}_{\mathrm{c,\,old}}\,\mathbf{u}_{\mathrm{b}} - \boldsymbol{\Psi}_{\mathrm{c,\,free}}\,\mathbf{u}_{\mathrm{b}}), \tag{26}$$

where $^{+}$ represents the generalised (pseudo) inverse. The above equation can be further simplified due to the properties of the fixed-interface modes $\boldsymbol{\Phi}_{\mathrm{i}}$, which

are the same for all three models (no-contact, continuous and penalty):

$$\boldsymbol{\Phi}^{+}_{\mathrm{i,\,new}}\boldsymbol{\Phi}_{\mathrm{i,\,old}} = \mathbf{I} \tag{27}$$

Eq. (26) can be written as:

$$\boldsymbol{\eta}_{\mathrm{i,\,new}} = \boldsymbol{\eta}_{\mathrm{i,\,old}} + \boldsymbol{\Phi}^{+}_{\mathrm{i,\,new}}\left(\boldsymbol{\Psi}_{\mathrm{c,\,old}} - \boldsymbol{\Psi}_{\mathrm{c,\,new}}\right)\mathbf{u}_{\mathrm{b}} \tag{28}$$

and if the boundary displacements $\mathbf{u}_{\mathrm{b}}$ are zero, the transformation is straightforward:

$$\boldsymbol{\eta}_{\mathrm{i,\,new}} = \boldsymbol{\eta}_{\mathrm{i,\,old}} \tag{29}$$

The above transformation is valid for all three possible cases (no-contact and continuous, penalty and no-contact as well as the penalty and continuous models) due to the definition of the constraint modes:

$$\boldsymbol{\Psi}_{\mathrm{c}} = -\mathbf{K}_{\mathrm{bi}}\,\mathbf{K}^{-1}_{\mathrm{ii}} \tag{30}$$

It is clear that the computation is independent of the $\mathbf{K}_{\mathrm{bb}}$ part, which is modified by the penalty method. Hence, the difference $\boldsymbol{\Psi}_{\mathrm{c,\,old}} - \boldsymbol{\Psi}_{\mathrm{c,\,new}}$ in Eq. (28) is $\mathbf{0}$ and therefore Eq. (28) is simplified to Eq. (29).

3.2.2 MacNeal and Rubin methods

The Rubin-method reduction matrix is given in Eq. (14). Comparing the new and old models' physical DoF (Eq. (24)) results in:

$$\begin{aligned}&\left(\boldsymbol{\Phi}_{\mathrm{rf|i,\,old}} - \boldsymbol{\Psi}_{\mathrm{r|i,\,old}}\,\mathbf{K}_{\mathrm{r,bb,\,old}}\,\boldsymbol{\Phi}_{\mathrm{rf|b,\,old}}\right)\boldsymbol{\eta}_{\mathrm{rf,\,old}} + \left(\boldsymbol{\Psi}_{\mathrm{r|i,\,old}}\,\mathbf{K}_{\mathrm{r,bb,\,old}}\right)\mathbf{u}_{\mathrm{b}} = \\ &\left(\boldsymbol{\Phi}_{\mathrm{rf|i,\,new}} - \boldsymbol{\Psi}_{\mathrm{r|i,\,new}}\,\mathbf{K}_{\mathrm{r,bb,\,new}}\,\boldsymbol{\Phi}_{\mathrm{rf|b,\,new}}\right)\boldsymbol{\eta}_{\mathrm{rf,\,new}} + \left(\boldsymbol{\Psi}_{\mathrm{r|i,\,new}}\,\mathbf{K}_{\mathrm{r,bb,\,new}}\right)\mathbf{u}_{\mathrm{b}}\end{aligned} \tag{31}$$

Note that we joined the rigid-body and free-interface modes into a joint vector $\boldsymbol{\eta}_{\mathrm{rf}} = \left[\boldsymbol{\eta}_{\mathrm{r}}\,\boldsymbol{\eta}_{\mathrm{rf}}\right]^{\mathrm{T}}$. Eq. (31) leads to the new coordinates (initial conditions) in the new modal space:

$$\begin{aligned}\boldsymbol{\eta}_{\mathrm{rf,\,new}} = &\left(\boldsymbol{\Phi}_{\mathrm{rf|i,\,new}} - \boldsymbol{\Psi}_{\mathrm{r|i,\,new}}\,\mathbf{K}_{\mathrm{r,bb,\,new}}\,\boldsymbol{\Phi}_{\mathrm{rf|b,\,new}}\right)^{-1}\Big(\\ &\left(\boldsymbol{\Phi}_{\mathrm{rf|i,\,old}} - \boldsymbol{\Psi}_{\mathrm{r|i,\,old}}\,\mathbf{K}_{\mathrm{r,bb,\,old}}\,\boldsymbol{\Phi}_{\mathrm{rf|b,\,old}}\right)\boldsymbol{\eta}_{\mathrm{rf,\,old}} + \\ &\left(\boldsymbol{\Psi}_{\mathrm{r|i,\,old}}\,\mathbf{K}_{\mathrm{r,bb,\,old}} - \boldsymbol{\Psi}_{\mathrm{r|i,\,new}}\,\mathbf{K}_{\mathrm{r,bb,\,new}}\right)\mathbf{u}_{\mathrm{b}}\Big)\end{aligned} \tag{32}$$

The above equation can be simplified for the no-contact and continuous models, since the free-interface modes are the same ($\boldsymbol{\Phi}_{\mathrm{rf|i,\,free}} = \boldsymbol{\Phi}_{\mathrm{rf|i,\,fixed}}$).

3.2.3 Dual Craig-Bampton method

The Dual Craig-Bampton reduction matrix is given in Eq. (15). A comparison of all the physical DoF ($\mathbf{u}_{\mathrm{old}} = \mathbf{u}_{\mathrm{new}}$) results in:

$$\boldsymbol{\Phi}_{\mathrm{rf,\,old}}\,\boldsymbol{\eta}_{\mathrm{rf,\,old}} + \boldsymbol{\Psi}_{\mathrm{r,\,old}}\,\mathbf{g}_{\mathrm{b}} = \boldsymbol{\Phi}_{\mathrm{rf,\,new}}\,\boldsymbol{\eta}_{\mathrm{rf,\,new}} + \boldsymbol{\Psi}_{\mathrm{r,\,new}}\,\mathbf{g}_{\mathrm{b}} \tag{33}$$

and leads to the new modal space coordinates:

$$\boldsymbol{\eta}_{\mathrm{rf,\,new}} = \boldsymbol{\Phi}^{-1}_{\mathrm{rf,\,new}}\left(\boldsymbol{\Phi}_{\mathrm{rf,\,old}}\,\boldsymbol{\eta}_{\mathrm{rf,\,old}} + \left(\boldsymbol{\Psi}_{\mathrm{r,\,old}} - \boldsymbol{\Psi}_{\mathrm{r,\,new}}\right)\mathbf{g}_{\mathrm{b}}\right) \tag{34}$$

The above equation can be further simplified for the no-contact and continuous models, since the free-interface modes are the same ($\boldsymbol{\Phi}_{\mathrm{rf|i,\,free}} = \boldsymbol{\Phi}_{\mathrm{rf|i,\,fixed}}$):

$$\boldsymbol{\eta}_{\mathrm{rf,\,free}} = \boldsymbol{\eta}_{\mathrm{rf,\,fixed}} + \boldsymbol{\Phi}_{\mathrm{rf,\,free}}^{-1} \left(\boldsymbol{\Psi}_{\mathrm{r,\,fixed}} - \boldsymbol{\Psi}_{\mathrm{r,\,free}} \right) \mathbf{g}_{\mathrm{b}} \tag{35}$$

3.3 Final remarks

The derivations of all the methods demonstrate that the Craig-Bampton method is the most straightforward. However, since the static and vibration modes are time-invariant and are only a function of the model, the initial condition coefficient matrices are determined only once during the preprocessing. Hence, the computation time is usually negligible in comparison to the integration time. Note, that in the case of multiple contact locations, the number of boundary DoF increases accordingly, as well as the complexity of the event structure and therefore the number of continuous and penalty models.

Note that the derived models are based on the classical linear model-reduction techniques and on a linear (penalty) contact model. In recent studies, for instance [29], newer non-linear contact models are proposed, which are capable of simulating more complex contact behaviours, such as different loading and unloading paths. The use of such models would require the use of non-linear model-reduction techniques [14], which certainly present challenging issues for further research in this field.

4 Case study

Ever-increasing operating speeds and the enforcement of lightweight designs often lead to excessive vibration and noise with modern machines. The vibration may result in different contact situations and changing boundary conditions during operation. Therefore, the natural frequencies of the system are not constant and can cause the extended resonance behaviour due to the closely spaced peaks of the fixed (in-contact) and free (no-contact) structure. This behaviour can be observed on various types of rotating machinery, e. g. , the instability of a washing machine during its spin cycle. In order to demonstrate the applicability of the developed method, a simple case study is presented. A clamped steel beam with a unilateral constraint is excited by a harmonic force at the free end. The system parameters are given in Table 1. The beam is discretized with 101 nodes using three DoF (x, y and φ) and has a unilateral constraint in the y-direction (see Fig. 4). Two different contact situations will be analysed. Firstly, the unilateral constraint will be considered at node 4 (Case 1) and secondly at node 13 (Case 2), as shown in Fig. 4.

Before the simulation, the modal reduction was applied using the Craig-Bampton method, as presented in Section 2. The reduction involves taking the first 10 fixed-interface modes and neglecting the higher modes. This reduces the model from 300 DOF to 12 DOF, consisting of 10 inner DOF and 2 boundary DOF: one for the constraint (4y/13y) and one for the excitation force (101y).

Table 1: Material properties.

Name	Symbol	Value
Length	l	500 mm
Width	w	10 mm
Height	h	5 mm
Young's modulus	E	2.1 MPa
Density	ρ	7850 kg/m^3
Poisson's ratio	μ	0.33
Penalty stiffness	k_{penalty}	5e9 N/m
Penalty damping	d_{penalty}	5e5 Ns/m

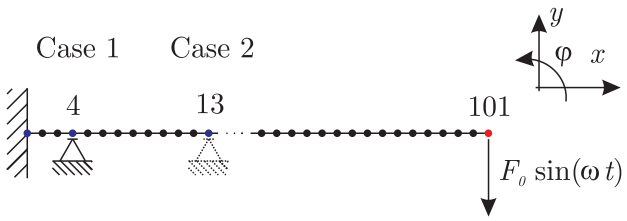

Figure 4: Numerical model of a clamped beam with a unilateral constraint.

The first ten natural frequencies for the case of the free (no-contact) and the fixed beam (continuous contact) are shown in Table 2. It is clear that the first

Table 2: First ten natural frequencies of the fixed and free beam.

Nat. freq. [Hz]	1	2	3	4	5	6	7	8	9	10
Free	33.45	209.24	584.06	1139.39	1872.69	2589.42	2778.07	3848.83	5077.51	6456.10
Fixed (4y)	35.21	220.57	616.45	1203.93	1980.75	2697.32	2940.96	4077.58	5382.72	6847.81
Fixed (13y)	41.06	258.92	726.9	1424.26	2347.65	2976.36	3487.45	4829.83	6350.88	7976.11

natural frequency of the free beam (33.45 Hz) is fairly close to the fixed case (35.21 Hz and 41.06 Hz).

The integration procedure (see Table 3) involves an event-driven integration, as proposed in section 3.

In total, the integration consists of three contact states (no-contact, continuous and penalty) and seven events. The event structure is shown in Fig. 5. Event 1 occurs when the constraint force (Eq. 22) in the continuous model is negative and the switch to the no-contact model occurs. Afterwards, Event 2 occurs when the no-contact model again reaches the constraint (displacement $x = 0$) and a transition to the penalty model occurs. Events 3, 4, 5, 6 and 7 serve for the purposes of the penalty model (shown in Fig. 3). Event 3 occurs after Event 2 if the amplitude of the relative velocity is within a user-defined tolerance ε. This prevents the numerical drift of velocities during integration. After Event 2 the transition to the Event 5 is also possible if the constraint

Table 3: Event-driven integration parameters.

Name	Symbol	Value
Integration time	t	0 - 50 s
Angular velocity	$\omega(t)$	$5\,t$ rad/s
Excitation force	$F(t)$	$100\sin(\omega(t)\,t)$ N
Integrator		Dopri [34, 35]
Maximum time step	$\Delta t_{\max}$	1e-3 s
Absolute tolerance		1e-12 s
Relative tolerance		1e-12
Event tolerance	ε	1e-12

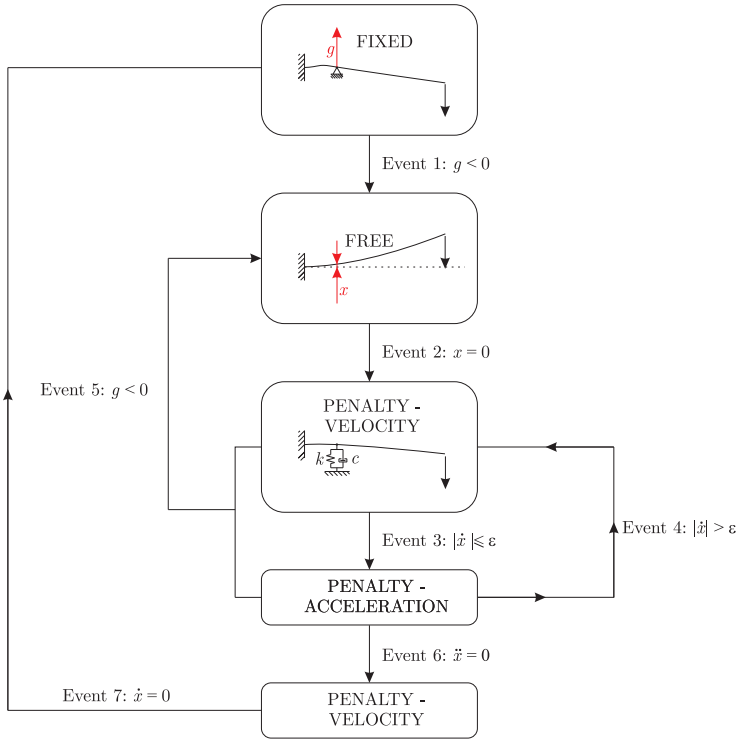

Figure 5: Identified events for a clamped beam structure.

force is negative. Hence, a switch to the no-contact model occurs. After Event 3 occurs either Event 4, Event 5 or Event 6 can occur. Event 4 occurs if the user-defined tolerance ε is exceeded and afterwards either Event 3 or 5 can occur. Event 6 occurs when the constraint acceleration is zero. This provides a confirmation that the velocity peak (local minima/maxima) is within the tolerance ε. Afterwards, a switch to the continuous model occurs and the constraint

velocities are set to zero.

The integration results in 520391 time points with the corresponding system response (12 DoF in reduced space) and takes approximately 2.5 h on a PC (2 Processors Intel Xeon CPU E5-2687W, 256 GB RAM). The results are expanded back to the physical space (300 DoF) with the help of the Craig-Bampton reduction matrix (see Eq. 4) and the displacements for Case 1 (point 101y) can be seen in Fig. 6a. Similar behaviour can be observed for Case 2 in Fig. 6b. The

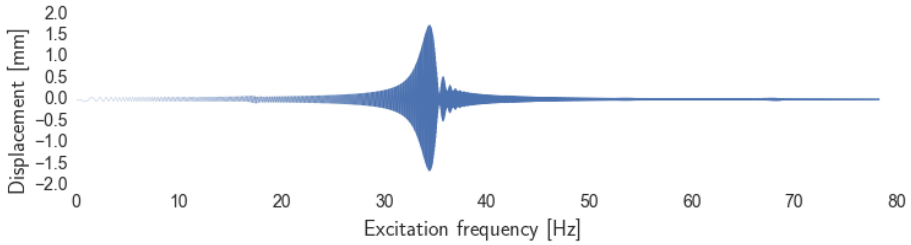

(a)

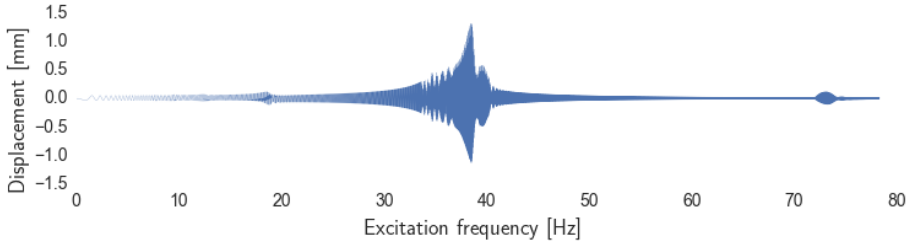

(b)

Figure 6: Time response at the free end (position 101y) of a clamped beam exposed to an excitation force: a) Case 1, b) Case 2.

peak at 35 Hz in Fig. 6a corresponds to the first natural frequencies of the continuous (35.21 Hz) and no-contact (33.45 Hz) states. Since the peaks are near to each another the resonance phase lasts slightly longer. A similar behaviour can be observed for Case 2 (Fig. 6b), where the two natural frequencies at 33.21 Hz and 41.06 Hz extend the resonance behaviour. A better representation of the mentioned phenomena can be observed in a spectrogram (see Fig. 7). In Fig. 7b the influence of the changing contact condition is very clearly seen in increased amplitudes during the excitation-frequency region between 33 Hz and 42 Hz.

In order to show the efficiency of the mixed contact model, a simulation with a pure penalty contact formulation was performed. In both cases the reduced basis was the same and only the contact formulation was different for both cases. By using the well-established pure penalty contact formulation, the computation time to simulate 50 s of system response takes approximately four times longer.

Finally, it can be concluded that the proposed numerical method offers an

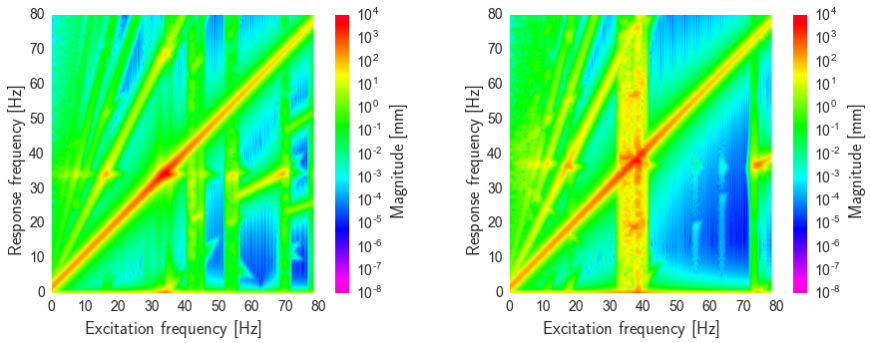

Figure 7: Spectrum at the free end (position 101y) of a clamped beam: a) Case 1, b) Case 2.

efficient and accurate procedure for the dynamics simulations of flexible bodies with unilateral contacts.

5 Conclusions

A new and efficient numerical procedure for modelling the dynamic response of linear-elastic systems with unilateral contacts is presented. Model-reduction techniques are applied in order to reduce the physical DoF, and with this the number of differential equations. Additionally, the contact formulation is based on a combination of single- and set-valued force laws with three main contact states: no-contact, continuous and impact/penalty. This formulation enables faster integration times than the pure-penalty method, since the added penalty weight is only used for impact contacts. The combination of model-reduction techniques and the mixed contact formulation is used within a proposed event-driven integration scheme. In order to efficiently combine both methods, an algorithm was developed to update the reduction basis and the initial conditions according to the contact state.

The applicability of the method is shown on a clamped beam with a unilateral contact and a harmonic force at the free end. The method can effectively detect extended resonance regions that occur due to the changing contact conditions. Moreover, the method offers the possibility to effectively model the dynamics response of flexible systems with unilateral contacts.

References

[1] F. Pfeiffer. *Mechanical System Dynamics*. Springer, Berlin, 2008.

[2] A. A. Shabana. *Computational Dynamics, 3rd Edition*. Wiley, Chichester, U.K., 1st edition, 2010.

[3] M. Geradin and A. Cardona. *Flexible Multibody Dynamics: A Finite Element Approach*. Wiley, New York, 1st edition, 2001.

[4] A. A. Shabana. *Dynamics of Multibody Systems*. Cambridge University Press, New York, 4th edition, sep 2013.

[5] F. Pfeiffer and C. Glocker. *Multibody Dynamics with Unilateral Contacts*, volume 1996. Springer-Verlag Wien, 1st edition, 1996.

[6] B. Besselink, U. Tabak, A. Lutowska, N. van de Wouw, H. Nijmeijer, D. J. Rixen, M. E. Hochstenbach, and W. H. A. Schilders. A comparison of model reduction techniques from structural dynamics, numerical mathematics and systems and control. *Journal of Sound and Vibration*, 332(19):4403–4422, 2013.

[7] M. C. C. Bampton and R. R. Craig Jr. Coupling of substructures for dynamic analyses. *AIAA Journal*, 6(7):1313–1319, 1968.

[8] R. H. MacNeal. A hybrid method of component mode synthesis. *Computers & Structures*, 1(4):581–601, 1971.

[9] S. Rubin. Improved Component-Mode Representation for Structural Dynamic Analysis. *AIAA Journal*, 13(8):995–1006, 1975.

[10] R. R. Craig and C.-J. Chang. On the use of attachment modes in substructure coupling for dynamic analysis. Technical report, 1977.

[11] D. J. Rixen. A dual Craig–Bampton method for dynamic substructuring. *Journal of Computational and Applied Mathematics*, 168(1–2):383–391, 2004.

[12] S. N. Voormeeren. *Dynamic Substructuring Methodologies for Integrated Dynamic Analysis of Wind Turbines*. PhD thesis, 2012.

[13] O. Weeger, U. Wever, and B. Simeon. On the use of modal derivatives for nonlinear model order reduction. *International Journal for Numerical Methods in Engineering*, 108(13):1579–1602, 2016.

[14] H. Festjens, G. Chevallier, and J.L. Dion. Nonlinear model order reduction of jointed structures for dynamic analysis. *Journal of Sound and Vibration*, 333(7):2100–2113, 2014.

[15] J. Slavič and M. Boltežar. Simulating Multibody Dynamics With Rough Contact Surfaces and Run-in Wear. *Nonlinear Dynamics*, 45(3-4):353–365, 2006.

[16] J. Slavič, M. D. Bryant, and M. Boltežar. A new approach to roughness-induced vibrations on a slider. *Journal of Sound and Vibration*, 306(3–5):732–750, 2007.

[17] C. Glocker. Formulation of spatial contact situations in rigid multibody systems. *Computer Methods in Applied Mechanics and Engineering*, 177(3–4):199–214, 1999.

[18] P. Lötstedt. Mechanical Systems of Rigid Bodies Subject to Unilateral Constraints. *SIAM Journal on Applied Mathematics*, 42(2):281–296, 1982.

[19] J. J. Moreau. Unilateral Contact and Dry Friction in Finite Freedom Dynamics. International Centre for Mechanical Sciences, pages 1–82. Springer Vienna, 1988.

[20] M. Jean. The non-smooth contact dynamics method. *Computer Methods in Applied Mechanics and Engineering*, 177(3-4):235–257, 1999.

[21] G. Čepon and M. Boltežar. Dynamics of a belt-drive system using a linear complementarity problem for the belt–pulley contact description. *Journal of Sound and Vibration*, 319(3–5):1019–1035, 2009.

[22] K. Willner. Elasto-Plastic Normal Contact of Three-Dimensional Fractal Surfaces Using Halfspace Theory. *Journal of Tribology*, 126(1):28, 2004.

[23] D. Goerke and K. Willner. Normal contact of fractal surfaces — Experimental and numerical investigations. *Wear*, 264(7):589–598, 2008.

[24] J.-P. Arz and F. Laville. Experimental characterization of small thickness elastomeric layers submitted to impact loading. *Journal of Sound and Vibration*, 326(1):302–313, 2009.

[25] K. H. Hunt and F. R. E. Crossley. Coefficient of Restitution Interpreted as Damping in Vibroimpact. *Journal of Applied Mechanics*, 42(2):440, 1975.

[26] R. Pohrt and V. L. Popov. Normal Contact Stiffness of Elastic Solids with Fractal Rough Surfaces. *Physical Review Letters*, 108(10):104301, 2012.

[27] C. Zhai, S. Bevand, Y. Gan, D. Hanaor, and G. Proust. Measurement of normal contact stiffness on fractal rough surfaces. In *23rd Australasian Conference on the Mechanics of Structures and Materials (ACMSM23), vol. II, Byron Bay, NSW, 9-12 December, Southern Cross University, Lismore, NSW*, pages 733–738, 2014.

[28] R. Kostek. The modelling of loading, unloading and reloading of the elastic-plastic contact of rough surfaces. *Journal of Theoretical and Applied Mechanics*, 50(2):509–530, 2012.

[29] Hamid Ahmadian and Mohsen Mohammadali. A distributed mechanical joint contact model with slip/slap coupling effects. *Mechanical Systems and Signal Processing*, 80(1):206–223, 2016.

[30] D. De Klerk, D. J. Rixen, and S. N. Voormeeren. General Framework for Dynamic Substructuring: History, Review and Classification of Techniques. *AIAA Journal*, 46(5):1169–1181, 2008.

[31] R. R. Craig and A. J. Kurdila. *Fundamentals of Structural Dynamics*. Wiley, Hoboken, N.J, 2nd edition, 2006.

[32] M. Geradin and D. J. Rixen. *Mechanical Vibrations: Theory and Application to Structural Dynamics*. Wiley, Hoboken, New Jersey, 3rd edition, 2015.

[33] R. Zander. *Flexible Multi-Body Systems with Set-Valued Force Laws*. PhD thesis, München, 2008.

[34] R. H. Clewley. Hybrid Models and Biological Model Reduction with PyDSTool. *PLOS Comput Biol*, 8(8):e1002628, 2012.

[35] R. H. Clewley, W. E. Sherwood, M. D. LaMar, and J. M. (2007) Guckenheimer. PyDSTool, a software environment for dynamical systems modeling.